Special Collection

Photopharmacology on Acetylcholinesterase: Novel Photoswitchable Inhibitors with Improved Pharmacological Profiles

Matthias Scheiner[+,a] Alexandra Sink[+,a] Philipp Spatz,[a] Erik Endres,[a] and Michael Decker*[a]

Considerable effort has previously been invested in a light-controlled inhibition of the enzyme acetylcholinesterase (AChE). We found that a novel azobenzene-based bistacrine AChE inhibitor switched faster than the known dithienylethene based bistacrine and inverted the photo-controlled interactions of the photoisomers compared to its dithienylethene congener. Furthermore, we have optimized a previously described light-controlled tacrine-based AChE inhibitor. Isomerization upon irradiation with UV light of the novel inhibitor was observed in aqueous medium and showed no fatigue over several cycles. The *cis*-enriched form showed an 8.4-fold higher inhibition of *h*AChE compared with its *trans*-enriched form and was about 30-fold more active than the reference compound tacrine with a single-digit nanomolar inhibition. We went beyond proof-of-concept to discover photoswitchable AChE inhibitors with pharmacologically desirable nanomolar inhibition, "*cis*-on" effect, and pronounces differences between the photoisomers.

1. Introduction

Irradiation by light can, among other things, influence the spatial arrangement of certain synthetic molecules. By incorporating light-sensitive moieties into a drug, biological processes can be light-controlled, since the isomerization can directly be translated into a change in affinity or pharmacological activity. This simple idea forms the cornerstone for an emerging field of pharmaceutical science, photopharmacology.[1] There are already numerous photoswitchable biologically active molecules known, targeting a wide variety of biomolecules.[2] Various light-sensitive moieties and strategies for incorporating those into drugs have been described.[3] All these photosensitive moieties have in common, that they exist in two different isomers, one of which is thermodynamically more favorable than the other. These moieties also differ in the isomerization wavelength, the stability of the thermodynamically less favorable form, their molecular weight and steric properties.[3a] Azobenzene and the dithienylethene (DTE) are the two best-described photoswitchable moieties for the design of photoswitchable drugs.

[a] *M. Scheiner,[+] A. Sink,[+] P. Spatz, E. Endres, Prof. Dr. M. Decker*
Pharmazeutische und Medizinische Chemie
Institut für Pharmazie und Lebensmittelchemie
Julius-Maximilians Universität Würzburg
Am Hubland, 97074 Würzburg (Germany)
E-mail: Michael.decker@uni-wuerzburg.de

[+] *Authors are ordered alphabetically and contributed equally to this work.*

Supporting information for this article is available on the WWW under https://doi.org/10.1002/cptc.202000119

An invited contribution to a Special Collection on Photopharmacology

More than 50 million people worldwide suffer from the most common form of dementia, Alzheimer's disease (AD).[4] AD is a neurodegenerative disease of the central nervous system, which symptomatically leads to memory loss and disturbance of cognitive functions like orientation and abilities to judge or to reason.[5] After decades of research, there is still no cure for AD and only symptomatic treatment for early stages of AD is available as pharmacotherapy.[6]

A variety of biochemical changes in the brain of AD patients take place like aggregation of amyloidß (Aß) and τ-proteins, oxidative stress and deficits of the neurotransmitter acetylcholine (ACh), which is directly linked to memory loss.[5a,b,6–7] The enzyme acetylcholinesterase (AChE) and its isoenzyme butyrylcholinesterase (BChE) catalyze the hydrolysis of ACh.[7b,8] AChE possesses two binding sites: the catalytic active site (CAS) located at the bottom of a gorge and the peripheral anionic site (PAS) located at the rim of the gorge.[8] Inhibition of AChE leads to an increase of ACh and thereby beneficial effects for symptomatic treatment of AD.[9] Also reduction of Aβ aggregation in presence of selective PAS binding inhibitors like propidium was described.[10] However, the precise mechanism, inhibition and function of PAS is still unclear.[11] Therefore, development of suitable tool compounds represent a promising strategy to study PAS inhibition in specific pharmacological models.[12] One approach is represented by the design of photoswitchable tool molecules, which have been successfully used to study other biological mechanism in a non-invasive manner.[13] Two inhibitors of AChE have been described in the literature, which use different photoswitchable moieties, azobenzene and dithienylethene (DTE), to control the inhibition of AChE by different means.[12a,14] To control the catalytic activity of AChE with light, tacrine (**1**), the first FDA approved drug for the treatment of AD, was linked to an azobenzene via an ethylene linker to obtain azo(2)tacrine **2**.[14] The incorporation of the azobenzene resulted in a considerably (15-fold) reduced

AChE inhibition compared to tacrine (**1**), but showed a slight difference in inhibition of AChE upon irradiation, with the *cis*-isomer **2b** being more effective.[14] Azo(2)tacrine **2** can be switched rapidly, but switching was not observed in aqueous media and showed photofatigue after several cycles.[14]

Efforts to develop more potent and effective AChE inhibitors based on a different pharmacological concept, i.e. the strategy of dual CAS and PAS interaction, led to the discovery of bis(7)tacrine **3**. Bis(7)tacrine **3** indeed showed a mixed-type inhibition mechanism and it was proven that it inhibits AChE-induced Aß aggregation.[15] The results obtained for bis(7) tacrine **3** led to the development of a DTE-based bistacrine **4**. The resulting DTE-bistacrine **4** showed similar extent of inhibition of AChE compared to bis(7)tacrine **3** and also between its two photoisomers (see Figure 1), but interaction of the inhibitor with the PAS can be light-controlled. The *ring-open* isomer **4a** shows a non-competitive inhibition mechanism, while the *ring-closed* isomer **4b** shows a competitive inhibition mechanism. Consequently, the *ring-open* isomer **4a** can inhibit AChE induced Aß aggregation significantly better compared to its photoisomer **4b**. Inhibitor **4** can also be switched in aqueous medium with irradiation lasting several minutes and requiring intense light (150 W) and UV-light (312 nm). The thermally less favorable *ring-closed* isomer is stable for several months, but inhibitor **4** decomposes after repeated switching cycles.[12a] Further photoswitchable AChE inhibitors are the subject of current research, but so far only moderate AChE inhibition and no difference between the photoisomers has been described.[16]

2. Results and Discussion

2.1. Design

Combining the described concepts of AChE inhibition and photopharmacology, we have designed and synthesized two photoswitchable tool-molecules to study AChE inhibition, especially with regard to PAS inhibition. Therefore, two different strategies have been pursued. First, an azobenzene-based bistacrine **5** was synthesized to improve the photoswitchable properties of DTE-bistacrine **4** replacing DTE by azobenzene (see Figure 1). Unsubstituted azobenzenes can be switched at 365 nm and less intense light[17] than DTE, allowing a greater variety of biological applications in a non-invasive manner, which is advantageous for tool-molecules. Furthermore, *cis*-/*trans*-isomerization is very fast, allowing a real-time analysis of AChE with its particularly fast kinetics.[14] Second and regarding *azo*-bistacrine **5**, the linker length required to reach the PAS from the CAS could be estimated from crystal structure 2CKM,[18] i.e. bistacrine **3** in complex with *tc*AChE (see Figure 2). In this crystal structure, the distance between the two nitrogen atoms delimiting the linker is 9.7 Å. Modelling **5b** by replacing the heptylene chain of **3** with a *cis*-azobenzene photoswitch results in a comparable distance of 9.9 Å. The model was built

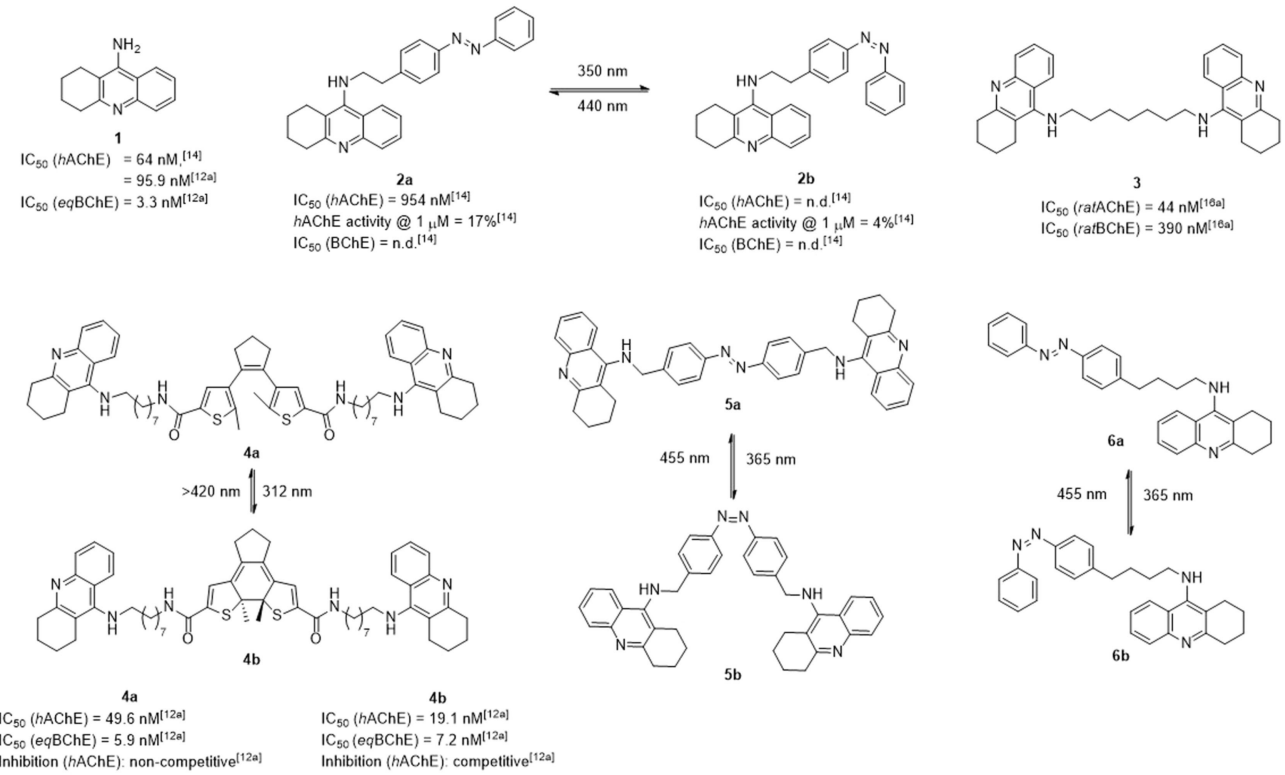

Figure 1. Tacrine (**1**),[12a,14] bis(7)tacrine **3**,[16a] derived photoswitchable inhibitors **2**,[14], **4**,[12a] and novel azobenzene-based inhibitors **5** and **6**, their photoisomers and their inhibitory activities at cholinesterases.

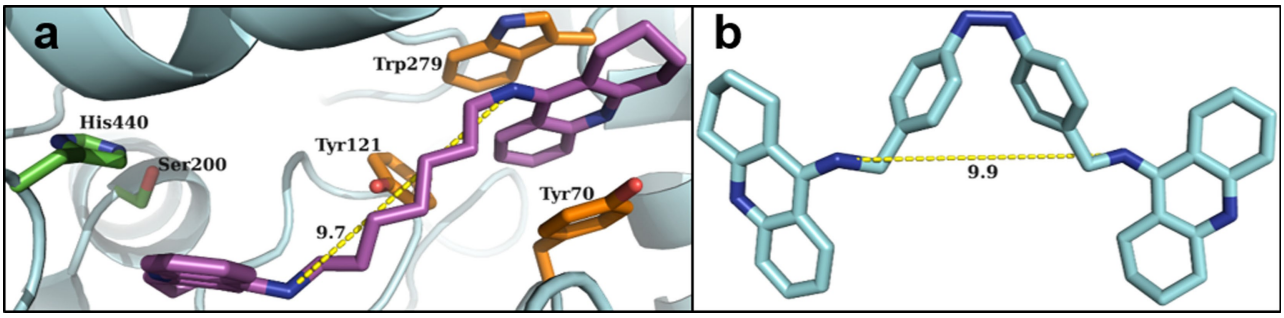

Figure 2. a) Binding mode of **3** in complex with *tc*AChE as observed in crystal structure 2CKM.[18] The residues of the CAS are marked green, PAS residues are shown in orange, ligand **3** is colored in purple. b) Model of **5b**. The distances indicated by the dotted yellow lines are given in Å.

after searching the Cambridge Structural Database (CSD) to derive average parameters for the C–N-N–C torsion angle (2°) and the angle between the plane of the azo-bond and the plane of the benzene unit (60°) of *cis*-azobenzenes.

Due to the length of the AChE gorge (approximately 20 Å[19]), it was likely that the linker of azo(2)tacrine **2** was too short to interact with the aromatic residues at the PAS, what we deemed necessary to increase K_i. We further rationalized this assessment based on the crystal structure 2CKM. Counting from the CAS-bound tacrine unit of bistacrine **3**, the fourth carbon atom of its alkyl chain reaches Tyr121, a residue contributing to the peripheral site.[19] Therefore, attaching the photoswitch to this atom should enable the benzene units of the switch to interact with the aromatic side chains of the PAS, such as Trp279 and Tyr70. To illustrate this, we modeled azo(4) tacrine **6a** in 2CKM. The ligand of the crystal structure was truncated after the fourth carbon atom. Then, the remaining atoms of the photoswitch were added. Subsequently, the new linker with tacrine was minimized, while keeping the C–N-N–C-torsion angle of the *trans*-photoswitch **6a** planar, in agreement with the CSD search results. Afterwards, the surrounding amino acids (Tyr121, Trp279 and Tyr70) were relaxed. Figure 3a shows, that the ligand fits into the PAS without significant changes in orientation of the side chains, underlining the plausibility of using a longer linker.

2.2. Synthesis

For synthesis of photoswitchable bistacrine **5**, synthesis started from 1-(bromomethyl)-4-nitrobenzene (**7**), the benzylic amine derivative **9** was synthesized in a Gabriel synthesis by reaction of cpd. **7** with potassium phthalimide to yield cpd. **8**, followed by hydrazinolysis. 9-Chloro-1,2,3,4-tetrahydroacridine (**10**) was synthesized according to a literature procedure and reacted in phenol and the presence of NaI with amine **9** to form tacrine-derivative **11**.[20] The moderate yield of 36% is due to the formation of tacrine (**1**) as by-product and associated difficulties in purification. The nitro moiety was reduced using Pd/C under hydrogen atmosphere to obtain aniline derivative **12**. Compound **12** decomposes to tacrine (**1**) in both MeOH and CH_2Cl_2 over time. To obtain azo-bistacrine **5**, cpd. **12** was therefore directly used in an oxidative homocoupling using NCS and DBU.[21] In this case, tacrine (**1**) was also formed as a by-product, which again led to difficulties in purification and therefore low yields (see Scheme 1).

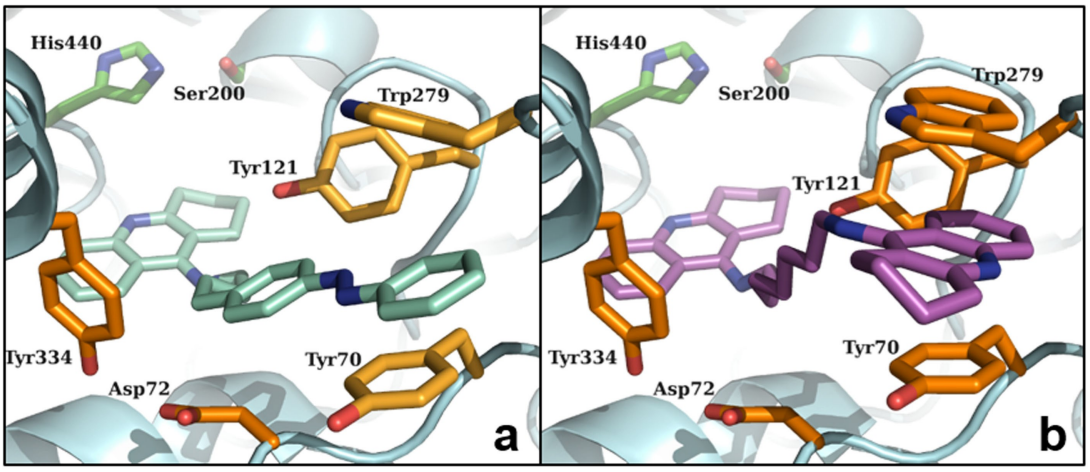

Figure 3. a) Model of azo(4)tacrine **6a** in complex with *tc*AChE derived from crystal structure 2CKM. The CAS residues are marked in green, the minimized residues of the PAS are shown in light orange, the unmodified residues in dark orange. b) For comparison, the crystal structure 2CKM with bis(7)tacrine **3** is shown from the same orientation as the model of **6a** in Figure 3a.[18]

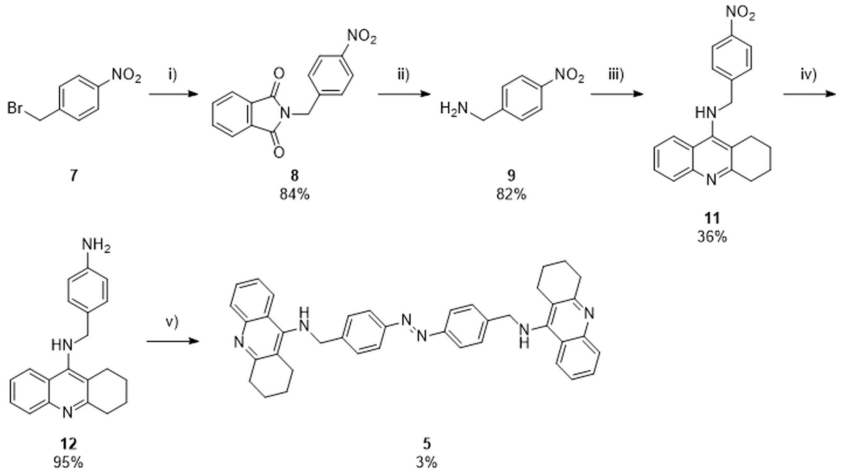

Scheme 1. Synthesis of azo-bistacrine **5**. Reagents and conditions: (i) potassium phthalimide, DMF, RT, 20 h; (ii) hydrazine hydrate, EtOH, −78 °C, 30 min; (iii) 9-Chloro-1,2,3,4-tetrahydroacridine (**10**), NaI, phenol, 180 °C, 2 h; (iv) Pd/C, H_2, MeOH, 10 bar, RT, 2 h; (v) NCS, DBU, CH_2Cl_2, −78 °C, 5 min.

Regarding the synthesis of azo(4)tacrine, in the first step commercially available 1-bromo-4-nitrobenzene (**13**) and but-3-yn-1-ol (**14**) were coupled to cpd. **15** in a Sonogashira reaction using CuI and $Pd(Cl_2)(Ph_3)_2$. The alkyne and nitro moieties were reduced in one step to cpd. **16**, using Pd/C under hydrogen atmosphere. By Mills reaction of the aniline derivative **16** with nitrosobenzene under acidic conditions, azoderivative **17** was formed. To interconvert the hydroxy moiety of **17** to amine **20**, first an Appel reaction using CBr_4 and PPh_3 was performed to obtain bromo derivative **18**, followed by substitution of the bromide with NaN_3 to azide derivative **19**, that was consequently reduced in a Staudinger reduction to **20** using PPh_3. To obtain azo(4)tacrine **6**, amine **19** reacted with 9-chloro-1,2,3,4-tetrahydroacridine (**10**) in phenol and in presence of NaI.[1] The seven-step synthesis sequence gave a high overall yield of 18% (see Scheme 2).

2.3. Photocharacterization

We investigated UV-vis absorption spectra of azobenzenes at a concentration of 25 μM (cpd. **5**) and 50 μM (cpd. **6**), respectively, in DMSO:H_2O (1:1). A strong π-π* transition band at short wavelengths ($\lambda(\pi\text{-}\pi^*) \approx 340$ nm) and a weaker n-π* band

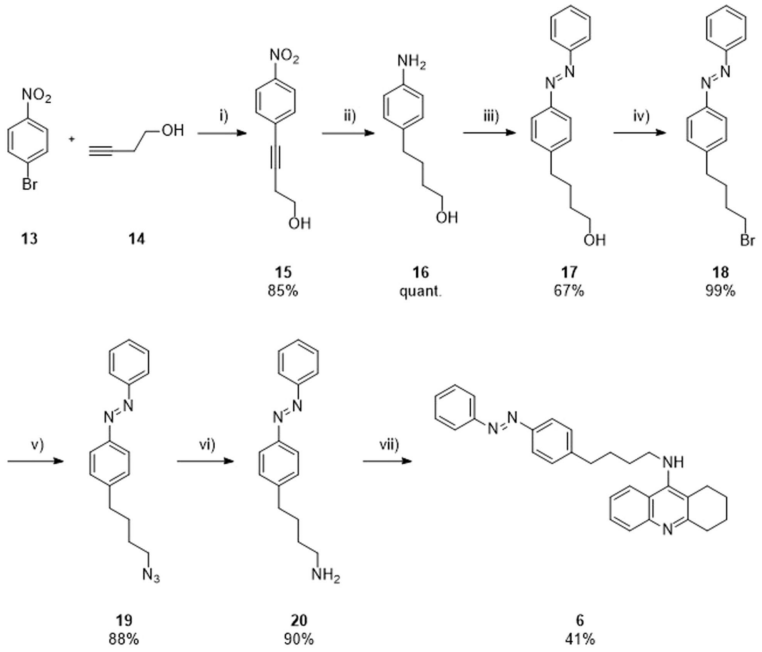

Scheme 2. Synthesis of azo(4)tacrine **6**. Reagents and conditions: (i) $Pd(Cl_2)(PPh_3)_2$, PPh_3, CuI, NEt_3:THF (3:2), RT, 15 h; (ii) Pd/C, H_2, MeOH, 10 bar, RT, 4 h; (iii) nitrosobenzene, AcOH, RT, 18 h; (iv) PPh_3, CBr_4, dry CH_2Cl_2, RT, 3 h; (v) NaN_3, dry DMF, 50 °C, 16 h; (vi) PPh_3, THF:H_2O (10:1), RT, 16 h; (vii) 9-Chloro-1,2,3,4-tetrahydroacridine (**10**), NaI, phenol, 180 °C, 2 h.

at higher wavelengths (λ(n-π*)$\approx$430 nm) were observed for both *trans*-photoisomers **5a** and **6a**. Irradiation with 365 nm and thereby photoconversion to *cis*, lead to a decrease in the absorption intensity of the π-π* transition band and an increase of the n-π* band with only minor changes in the wavelengths (1–2 nm) of the respective bands (see Table 1 and Figure 4).

The *cis*/*trans*-ratio was determined by HPLC analysis with detection at the respective isosbestic point and confirmed an excess of *cis*-isomers **5b** and **6b** after irradiation with 365 nm (see Table 1, Figure S1).

Maximum isomerization of azo(4)tacrine **6** was obtained by irradiation with 365 nm after $<$10 s and showed no fatigue after 9 cycles of isomerization with the *cis*-isomer **6b** being stable for at least 16 h at 25 °C in the dark (see Figure 4). Switching in cholinesterase assay buffer was confirmed (see **Figure S2**). Irradiation at 365 nm led to time-dependent linear decomposition of azo-bistacrine **5** in cholinesterase buffer (see **Figure S3**). Photocharacterization of **5** was therefore only carried out in H_2O:DMSO (1:1) and showed similar behavior as azo(4)tacrine **6** (see **Figure S4**). For testing cholinesterase inhibitory properties of **5** in a modified Ellmann's assay, a stock solution in DMSO was fist irradiated with 365 nm for an adapted time, and then diluted in the dark with assay buffer. Under these conditions it could be shown, that **5b** remains stable for hours (see **Figure S5**). This behavior has also to be taken into account when interpreting the published data on azo(2)tacrine **2** and potentially applying this compound to a pharmacological assay.[14]

Table 1. Photophysicochemical properties of azo-bistacrine **5** and azo(4)-tacrine **6**.

Compound	*trans*[a] λ_{max} (π-π*) [nm]	λ_{max} (n-π*) [nm]	*cis*[b] λ_{max} (n-π*) [nm]	PSS_{trans} (%)	PSS_{cis} (%)	$t_{1/2}$ (*cis*) [h]
azo-bistacrine **5**	353	429	430	90	86	$>$15 h
azo(4)tacrine **6**	338	431	433	80	63	$>$15 h

[a] Mixture of both photoisomers at dark state (*trans*-enriched). [b] Mixture of both photoisomers after irradiation at 365 nm (*cis*-enriched). λ_{max} (π-π*, n-π*) is the wavelength at the maximal absorption of the π-π* and n-π* transition bands, respectively. Photostationary state (PSS) percentages at dark state and after irradiation with 365 nm for *cis* were determined using HPLC at the isosbestic point.

2.4. Enzyme Inhibition

Both inhibitors **5** and **6** show more pronounced inhibition of *h*AChE compared to tacrine (**1**). Photoisomers of azo-bistacrine **5** show single-digit nanomolar inhibition of *h*AChE with no significant difference between its photoisomers and a similar selectivity towards *h*AChE over the isoenzyme *h*BChE by a factor of about five. For azo(4)tacrine **6**, the isomerization is translated into an 8.4-fold difference in inhibition, with a single-digit nanomolar IC_{50} of the *cis*-enriched form **6b** at *h*AChE. Additionally, both isomers show selectivity towards *h*AChE, which is very pronounced for the *cis*-enriched form **6b** with a factor of 70 (see Table 2).

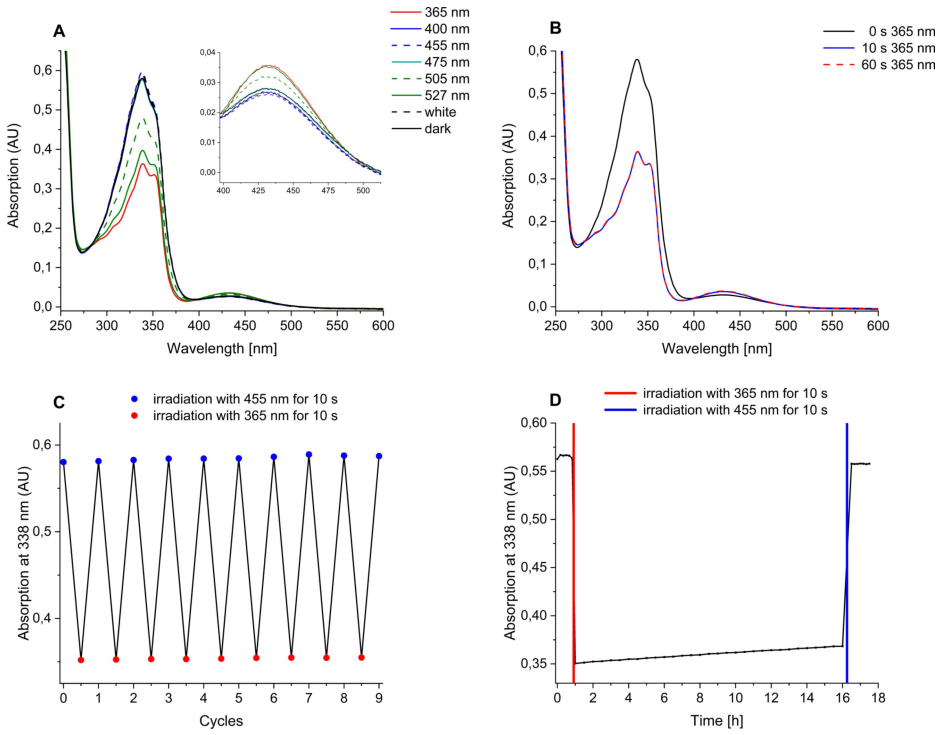

Figure 4. Photochemical properties of azo(4)tacrine **6**. Absorption spectrum of compound **6** a) in the dark and after 10 s irradiation with different wavelength; b) in the dark and after different irradiation at 365 nm; c) repeatedly isomerization by irradiation with 365 nm and 455 nm for 10 s; d) stability of compound **6b** in the dark. Experiments were performed in H_2O:DMSO (1:1) at 25 °C with 50 µM **6**.

Table 2. Inhibition results of literature known inhibitors **1**–**4** and photoisomers of **5** and **6** on *h*AChE and *h*BChE.

		IC_{50} (AChE) [nM] ($pIC_{50} \pm SEM$, n = 3)	$IC_{50}(trans)$[a] /$IC_{50}(cis)$[b]	Hill slope (*h*AChE)	IC_{50} (*h*BChE) [nM] ($pIC_{50} \pm SEM$, n = 3)	$IC_{50}(trans)$[a] /$IC_{50}(cis)$[b]
1	tacrine	111 (6.96 ± 0.02)	n.d.	0.9	54.0 (7.37 ± 0.02)	n.d.
2a	*trans*-azo(2)tacrine[a]	954[c][14]	n.d.[14]	n.d.[14]	n.d.[14]	n.d.[14]
2b	*cis*-azo(2)tacrine[b]	n.d.[14]		n.d.[14]	n.d.[14]	
3	bis(7)tacrine	44[d][16a]	n.d.[16a]	n.d.[16a]	340[e][16a]	n.d.[16a]
4a	*open*-DTE-bistacrine	49.6[c][12a]	2.60[f][12a]	1.6[12a]	5.9[g][12a]	0.819[f][12a]
4b	*closed*-DTE-bistacrine	19.1[c][12a]		1.2[12a]	7.2[g][12a]	
5a	*trans*-azo-bistacrine[a]	6.18[c] (8.21 ± 0.01)	1.24	0.9	35.7[h] (7.47 ± 0.04)	1.12
5b	*cis*-azo-bistacrine[b]	4.97[c] (8.31 ± 0.01)		0.9	32.0[h] (7.49 ± 0.03)	
6a	*trans*-azo(4)tacrine[a]	34.1[c] (7.47 ± 0.06)	8.40	0.8	664[h] (6.18 ± 0.02)	2.31
6b	*cis*-azo(4)tacrine[b]	4.06[c] (8.39 ± 0.15)		0.6	287[h] (6.54 ± 0.02)	

[a] Mixture of both photoisomers at dark state (*trans*-enriched). [b] Mixture of both photoisomers after irradiation at 365 nm (*cis*-enriched). [c] *h*AChE human recombinant, expressed in HEK 293 cells. [d] *rat*AChE. [e] *rat*BChE. [f] IC_{50}(*ring-open*)/IC_{50}(*ring-closed*). [g] *eq*BChE. [h] *h*BChE from human serum.

The mode of inhibition of compounds **5** and **6** was analyzed according to literature known procedures by recording substrate-velocity curves in the presence of different inhibitor concentrations (see Figure 5).[12a,22] For better illustration the Michaelis-Menten graphs were converted to Lineweaver-Burk plots, in which the reciprocal rates are plotted versus reciprocal substrate concentrations. The mode of inhibition was evaluated by comparison of the observed Lineweaver-Burk plots with theoretical trends for competitive, noncompetitive and mixed-type inhibition.[23] While increasing the concentration of inhibitor **5a**, the v_{max} value (reciprocal of the Y-intercept) remains the same, whereas the K_M value (negative reciprocal of the X-intercept) increases, which is typical for a competitive inhibitor.[12a,22] In contrary, the Lineweaver burk plot of the **5b** illustrates a non-competitive binding mode as the v_{max} value decreases with increasing inhibitor concentration, whereas K_M stays the same. This indicates that **5a** binds competitively to CAS of *h*AChE, whereas upon irradiation bistacrine **5b** binds non-competitively to a different binding site, possibly PAS. The *trans*-isomer of azo(4)tacrine **6a** binds competitively to CAS, indicated by a constant v_{max} value and increased K_M value. On the contrary, the *cis*-enriched form **6b** is a mixed-type inhibitor as the v_{max} value decreases and K_M increases with increasing inhibitor concentration. This can be explained by simultaneously binding with the CAS and the PAS of *h*AChE.

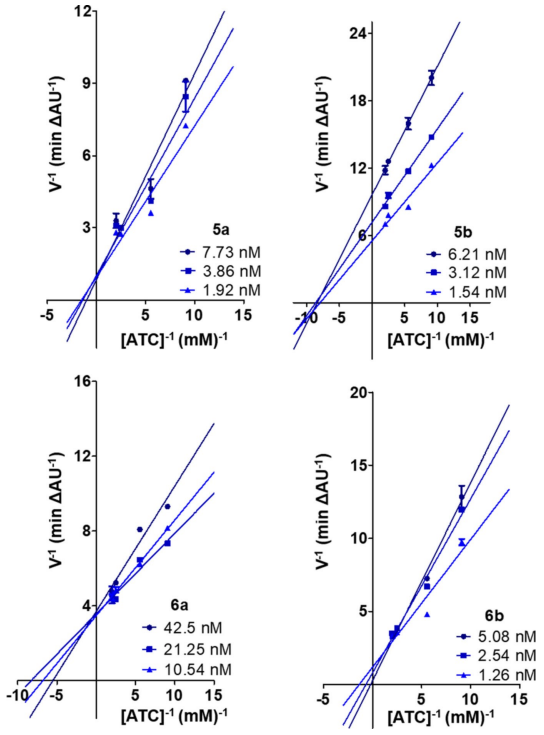

Figure 5. Kinetic study on the mechanism of *h*AChE inhibition by photoisomers of **5** and **6**. Lineweaver–Burk plots of *h*AChE with different acetylthiocholine (ATC) concentrations in the presence of increasing inhibitor concentrations.

3. Conclusion

Exchange of DTE by azobenzene as photoswitchable moiety in a bistacrine improves the photochemical properties of this tool molecule: Switching can be performed in less than 10 s, at 365 nm and can be repeated over many cycles without any photofatigue. Additionally, pharmacological properties were further improved as both isomers of the azobenzene-based bistacrine **5** are one-digit nanomolar and selective *h*AChE inhibitors. Upon irradiation with light the mechanism of inhibition can be changed from competitive **5a** (*trans*-enriched) to non-competitive **5b** (*cis*-enriched), strongly indicating a PAS interaction in accordance with the design based on the x-ray structure. This "*cis*-on" PAS inhibition provides many advantages for further pharmacological applications. However, photofatigue in buffer solution upon irradiation might limit biological applications.

In addition, we were able to show that the linker length of the photoswitchable moiety to tacrine has enormous influence not only on the biological interaction, but also on the physicochemical properties of the compound, since extending linker length between tacrine (**1**) and azobenzene in azo(4) tacrine **6** led to improved photochemical properties, as switching was stable in aqueous medium and showed no photofatigue over several cycles. Furthermore, both photoisomers of azo(4)tacrine **6** show a significantly higher inhibition and selectivity towards *h*AChE than azo(2)tacrine **2** and tacrine (**1**) itself. Hereby, the *cis*-enriched form **6b** is by a factor larger than eight more active than the thermodynamically more stable *trans*-isomer **6a**, so that inhibition of *h*AChE can be switched on by light. Possible hepatotoxic side effects of azo(4) tacrine **6** due to the incorporation of tacrine (**1**) might be reduced, since this effect is dose-dependent and photoisomer **6b** is almost 30-fold more effective compared to tacrine (**1**) resulting in a lower dosage.[23] As the photoisomer **6b** is a mixed-type inhibitor with PAS interaction, the mechanism of PAS interaction and other pharmacological applications regarding AChE can be evaluated with this tool molecule.

Experimental Section

Modelling

Modelling of *azo*-bistacrine **5b** was performed with MOE v. 2019.0102.[24] The Cambridge Structural Database was searched with ConQuest v. 2.0.5[25] to derive average parameters for the C–N-N–C torsion angle of the azo-unit and the angle described by the plane of the azo bond and the plane of the benzene unit of *cis*-azobenzenes.

Crystal structure 2CKM was also utilized to estimate a reasonable linker length for **6**. The *trans*-isomer **6a** was modelled into the binding pocket using MOE by truncating the original ligand after the fourth carbon atom and adding the remaining atoms of the photoswitch. Subsequently, the new linker with tacrine was minimized to a gradient of 0.001 kcal/(mol Å) using MMFF94x, while keeping the C–N–N–C-torsion angle of the *trans*-photoswitch planar, in agreement with the ConQuest search results. Afterwards, the surrounding amino acids (Tyr121, Trp279 and Tyr70) were relaxed using the Amber14 forcefield in MOE.

All figures were produced using Pymol.[26]

Reagents and Solvents

All reagents were used without further purification and were bought from common commercial suppliers, mainly Sigma Aldrich and Fluorochem. For anhydrous reaction conditions, anhydrous dimethylformamide was bought from Sigma Aldrich. Under argon atmosphere THF was dried prior to using by refluxing over sodium with benzophenone as an indicator. Dichloromethane was predried over calcium hydride and then distilled under argon atmosphere.

NMR Spectroscopy

Measurements of NMR spectra were performed on an Advance 400 of *Bruker* (^{1}H-NMR: 400 MHz, ^{13}C-NMR: 100 MHz). ^{1}H- and ^{13}C-NMR, DEPT135 and HSQC spectra were calibrated with the hydrogen signal of the respective solvent as an internal standard. In this work $CDCl_3$, CD_3OD and $(CD_3)_2SO$ were used as solvents (^{1}H: $CDCl_3$: 7.26 ppm, ^{1}H: CD_3OD: 3.31 ppm, ^{1}H: $(CD_3)_2SO$: 2.50 ppm; ^{13}C: $CDCl_3$: 77.16 ppm, ^{13}C: CD_3OD: 49.00 ppm, ^{13}C: $(CD_3)_2SO$: 39.52 ppm). *J* is the coupling constant in hertz [s^{-1}]. The abbreviations of the indicated signal diversities were: s = singlet, d = doublet, t = triplet, q = quartet, m = multiplet.

Liquid Chromatography Mass Spectrometry (LC-MS)

Measurements for verification and purity of the compounds were performed by LC-MS (from *Shimadzu*), comprising a DGU-20A3R controller, a pump LC-20AB, a degasser DGU-20A and a SPD-20A UV/Vis detector. ESI ionization was accomplished by LC-MS-2020 Single Quadrupol Mass Spectrometer. As stationary phase for analytical purpose a Synergi 4U fusion-RP 80 Å (150 × 4.6 mm) column was used. As mobile phase a gradient of H_2O/MeOH (both containing 0.1 % formic acid) (phase A/phase B) was used. The compounds were dissolved in MeOH and filtered through syringe filters.

Method

Flow rate: 1.0 mL/min; Detection: 254 nm;

Scan range: 100–1000 *m/z*;

Gradient: A: H_2O (0.1 % HCOOH); B: MeOH (0.1 % HCOOH)

0–8 min 5 %→90 % B, 8–13 min 90 % B, 13–14 min 90 %→5 % B, 14–18 min 5 % B

Melting Points

Melting points were measured with OptiMelt MPA-100 – automated melting point system from Stanford Research Systems. The device records a melting curve with sigmoidal trend, whereby the inflection point is reported as the melting point.

Synthesis

N,N′-((Diazene-1,2-diylbis(4,1-phenylene))bis(methylene))bis (1,2,3,4-tetrahydroacridin-9-amine) (5)

N-(4-Aminobenzyl)-1,2,3,4-tetrahydroacridin-9-amine (**12**) (205 mg, 0.676 mmol) was dissolved in CH_2Cl_2 (130 mL). DBU (202 µL, 1.35 mmol) was added and the mixture was stirred for 10 min at RT. After cooling down to −78 °C, NCS (181 mg, 1.35 mmol) was added. After 10 min the mixture was allowed to warm up and was quenched with sat. $NaHCO_{3\ aq}$. The layers were separated and the organic layer was washed with sat. $NaHCO_{3\ aq}$, H_2O and extracted with 1 M HCl. The aqueous layer was basified with 2 M NaOH and extracted with CH_2Cl_2 . The organic layers were washed with brine and dried over Na_2SO_4. The solvent was removed under reduced pressure. The crude product purified using preparative TLC (CH_2Cl_2:MeOH:NEt_3 (10:1:0.1) to obtain *N,N′*-((diazene-1,2-diylbis(4,1-phenylene))bis(methylene))bis(1,2,3,4-tetrahydroacridin-9-amine)) (**5**) (13.3 mg, 22.0 µmol, 3 %) as orange solid. Mp: degradation at 228 °C. LC-MS analysis: t_r = 8.29 min, ESI-MS: *m/z* calcd for $C_{40}H_{39}N_6$ $[M+H]^+$: 603.33, found 302.39 $[M+2H]^{2+}$.^{1}H-NMR (400 MHz, $CDCl_3$): δ = 8.03–7.90 (m, 8H, CH), 7.61–7.55 (m, 2H, CH), 7.50 (d, *J* = 8.2 Hz, 4H, CH), 7.36 (t, *J* = 7.6 Hz, 2H, CH), 4.69 (d, *J* = 6.4 Hz, 4H, CH_2), 4.24–4.18 (m, 2H, NH), 3.08 (t, *J* = 6.1 Hz, 4H, CH_2), 2.68 (t, *J* = 6.0 Hz, 4H, CH_2), 1.96–1.81 (m, 8H, CH_2) ppm. ^{13}C-NMR (100 MHz,

$CDCl_3$): δ = 159.0 (2C, C_q), 152.3 (2C, C_q), 150.2 (2C, C_q), 147.8 (2C, C_q), 143.1 (2C, C_q), 129.2 (2C, CH), 128.6 (2C, CH), 128.4 (4C, CH), 124.3 (2C, CH), 123.5 (4C, CH), 122.7 (2C, CH), 120.6 (2C, C_q), 117.4 (2C, C_q), 53.3 (2C, CH_2), 34.3 (2C, CH_2), 25.0 (2C, CH_2), 23.1 (2C, CH_2), 22.9 (2C, CH_2) ppm.

N-(4-(4-(Phenyldiazenyl)phenyl) butyl)-1,2,3,4-tetrahydroacridin-9-amine (6)

4-(4-(Phenyldiazenyl)phenyl)butan-1-amine (**20**) (100 mg, 0.395 mmol), 9-chloro-1,2,3,4-tetrahydroacridine (**10**) (85.7 mg, 0.395 mmol), NaI (14.8 mg, 99.4 μmol) and phenol (1.50 g) were mixed and heated to 180 °C for 2 h. The solvent was evaporated under reduced pressure and the crude product was purified using column chromatography (CH_2Cl_2:MeOH:NH_3 (100 : 1 : 0.1)→(20 : 1 : 0.1))) to obtain *N*-(4-(4-(phenyldiazenyl)phenyl) butyl)-1,2,3,4-tetrahydroacridin-9-amine (**6**) (70 mg, 0.162 mmol, 41 %) as brown oil. LC-MS analysis: t_r = 9.47 min, ESI-MS: *m/z* calcd for $C_{29}H_{31}N_4$ $[M+H]^+$: 435.36, found 435.25. ^{1}H-NMR (400 MHz, $CDCl_3$): δ = 8.34 (d, *J* = 8.5 Hz, 1H, CH), 8.18 (d, *J* = 8.6 Hz, 1H, CH), 7.89 (d, *J* = 7.1 Hz, 2H, CH), 7.81 (d, *J* = 8.2 Hz, 2H, CH), 7.60 (t, *J* = 7.6 Hz, 1H, CH), 7.54–7.44 (m, 3H, CH), 7.41–7.33 (m, 1H, CH), 7.30 (s, 1H, CH), 7.28 (d, *J* = 2.5 Hz, 1H, CH), 6.60 (s, 1H, NH), 3.92 (d, *J* = 6.6 Hz, 2H, CH_2), 3.18 (t, *J* = 5.7 Hz, 2H, CH_2), 2.75 (t, *J* = 7.12 Hz, 2H, CH_2), 2.63–2.57 (m, 2H, CH_2), 1.89–1.76 (m, 8H, CH_2) ppm. ^{13}C-NMR (100 MHz, $CDCl_3$): δ = 155.6 (1C, C_q), 152.6 (1C, C_q), 151.21 (1C, C_q), 151.18 (1C, C_q), 145.0 (1C, C_q), 138.8 (1C, C_q), 132.2 (1C, CH), 130.9 (1C, CH), 129.108 (2C, CH), 129.106 (2C, CH), 125.1 (1C, CH), 124.4 (1C, CH), 123.0 (2C, CH), 122.7 (2C, CH), 120.6 (1C, CH), 115.8 (1C, C_q), 110.9 (1C, C_q), 48.1 (1C, CH_2), 35.2 (1C, CH_2), 30.4 (1C, CH_2), 28.3 (1C, CH_2), 28.1 (1C, CH_2), 23.9 (1C, CH_2), 21.9 (1C, CH_2), 20.6 (1 C, CH_2) ppm.

2-(4-Nitrobenzyl)-2λ^4-isoindoline-1,3-dione (8)

4-Nitrobenzylbromid (**7**) (5.00 g, 23.1 mmol) was added to potassium phthalimide (4.29 g, 23.1 mmol) in DMF (110 mL). The reaction was stirred for 20 h. After filtration, the filtrate was concentrated *in vacuo*. The crude product was dissolved in CH_2Cl_2, washed with H_2O and dried over Na_2SO_4. 2-(4-Nitrobenzyl)-2λ^4-isoindoline-1,3-dione (**8**) (5.46 g, 19.2 mmol, 84 %) was obtained as a colorless solid. Mp: 165 °C. LC-MS analysis: t_r = 9.60 min, ESI-MS: m/z calcd for $C_{15}H_{11}N_2O_4$ $[M+H]^+$: 283.07, not found. ^{1}H-NMR (400 MHz, $CDCl_3$): δ = 8.20–8.15 (m, 2H, CH), 7.89–7.84 (m, 2H, CH), 7.77–7.71 (m, 2H, CH), 7.61–7.55 (m, 2H, CH), 4.93 (s, 2H, CH_2) ppm. ^{13}C-NMR (100 MHz, $CDCl_3$): δ = 167.9 (2C, C_q), 147.7 (1C, C_q), 143.4 (1C, C_q), 134.5 (2C, CH), 132.0 (2C, C_q), 129.5 (2C, CH), 124.1 (2C, CH), 123.8 (2C, CH), 41.0 (1C, CH_2) ppm.

4-Nitrobenzylamine (9)

2-(4-Nitrobenzyl)-2λ^4-isoindoline-1,3-dione (**8**) (1.99 g, 7.04 mmol) was dissolved in EtOH (60 mL). Hydrazine·hydrate (6 mL) was added. The reaction mixture was refluxed for 30 min. After cooling down to RT, sat. $NaHCO_{3\ aq}$ was added and the product was extracted with CH_2Cl_2. The combined organic layers were washed with H_2O, brine and dried over Na_2SO_4. The crude product was purified using column chromatography (CH_2Cl_2:MeOH:NH_3 (40 : 1 : 0.1)) to obtain 4-nitrobenzylamine (**9**) (877 mg, 5.77 mmol, 82 %) as a brown solid. Mp: 97 °C. LC-MS analysis: t_r = 3.41 min, ESI-MS: *m/z* calcd for $C_7H_9N_2O_2$ $[M+H]^+$: 153.07, found 153.15. ^{1}H-NMR (400 MHz, CD_3OD): δ = 8.72 (d, *J* = 8.7 Hz, 2H, CH), 8.18 (d, *J* = 8.5 Hz, 2H, CH), 5.27 (s, 2H, CH_2) ppm. ^{13}C-NMR (100 MHz, CD_3OD): δ = 151.1 (1C, C_q), 148.0 (1C, C_q), 129.2 (2C, CH), 124.5 (2C, CH), 45.9 (1C, CH_2) ppm.

9-Chloro-1,2,3,4-tetrahydroacridine (10)[20]

9-Chloro-1,2,3,4-tetrahydroacridine (**10**) was synthesized according to a literature procedure.[20] Briefly, anthranilic acid (2.45 g, 17.9 mmol) and cyclohexanone (2.04 mL, 19.7 mmol) were combined, $POCl_3$ (20 mL) was added and the mixture was heated for 1.5 h to 120 °C. The reaction mixture was cooled down to 0 °C and NH_3(25 $\%_{aq}$) was added dropwise. After quenching of $POCl_3$, EtOAc and H_2O were added, and the layers were separated. The aqueous layer was 3× extracted with EtOAc, organic layers were combined, dried over anhydrous $MgSO_4$ and concentrated *in vacuo*. The crude product was recrystallized twice from acetone to afford 9-chloro-1,2,3,4-tetrahydroacridine (**10**) (2.46 g, 17.9 mmol, 63 %) as a brown solid. Mp: 66 °C. LC-MS analysis: t_r = 9.95 min, ESI-MS: *m/z* calcd for $C_{13}H_{13}ClN$ $[M+H]^+$: 218.07, found, 218.03.^{1}H NMR (400 MHz, $CDCl_3$): δ = 8.15 (d, J = 8.4, 1H), 8.00 (d, J = 8.5 Hz, 1H), 7.70–7.64 (m, 1H), 7.54–7.52 (m, 1H), 3.15 (t, J = 5.6 Hz, 2H), 3.04 (t, J = 6.4 Hz, 2H), 1.99–1.95 (m, 4H) ppm. ^{13}C NMR (101 MHz, $CDCl_3$): δ = 159.4, 146.3, 141.8, 129.4, 128.9, 128.3, 126.6, 125.4, 123.7, 33.9, 27.5, 22.7, 21.5 ppm.

N-(4-Nitrobenzyl)-1,2,3,4-tetrahydroacridin-9-amine (11)

4-Nitrobenzylamine (**9**) (500 mg, 3.29 mmol), 9-chloro-1,2,3,4-tetrahydroacridine (**10**) (714 mg, 3.29 mmol), sodium iodide (123 mg, 0.823 mmol) and phenol (2.28 g) were mixed and stirred at 180 °C for 2 h. After cooling down, EtOAc was added. After filtration, the precipitation was washed with EtOAc. The crude product was purified using column chromatography (CH_2Cl_2:MeOH:NH_3 (30 : 1 : 0.1)→(20 : 1 : 0.1)) to obtain *N*-(4-nitrobenzyl)-1,2,3,4-tetrahydroacridin-9-amine (**11**) (394 mg, 1.18 mmol, 36 %) as brown oil. LC-MS analysis: t_r = 7.64 min, ESI-MS: *m/z* calcd for $C_{20}H_{20}N_3O_2$ $[M+H]^+$: 334.16, found 334.20. ^{1}H-NMR (400 MHz, CD_3OD): δ = 8.26 (d, J = 8.7 Hz, 2H, CH), 8.15 (d, J = 8.8 Hz, 1H, CH), 7.84–7.77 (m, 2H, CH), 7.66 (d, J = 8.6 Hz, 2H, CH), 7.44 (m, 1H, CH), 5.25 (s, 2H, CH_2), 3.06 (m, 2H, CH_2), 2.84–2.74 (m, 2H, CH_2), 1.98 (m, 4H, CH_2) ppm. ^{13}C-NMR (100 MHz, CD_3OD): δ = 159.2 (1C, C_q), 158.7 (1C, C_q), 157.9 (1C, C_q), 153.3 (1C, C_q), 147.2 (1C, C_q), 133.9 (1C, CH), 128.7 (2C, CH), 126.5 (1C, CH), 125.9 (1C, CH), 125.1 (2C, CH), 120.9 (1C, CH), 114.4 (1C, C_q), 114.1 (1C,C_q), 51.2 (1C, CH_2), 29.8 (1C, CH_2), 25.1 (1C, CH_2), 23.0 (1C, CH_2), 21.9 (1C, CH_2) ppm.

N-(4-Aminobenzyl)-1,2,3,4-tetrahydroacridin-9-amine (12)

N-(4-Nitrobenzyl)-1,2,3,4-tetrahydroacridin-9-amine (**11**) (269 mg, 0.807 mmol) was dissolved in MeOH (30 mL). The mixture was stirred over Pd/C under H_2 (10 bar) for 1.5 h. The mixture was filtrated over celite and the solvent was evaporated under reduced pressure. *N*-(4-aminobenzyl)-1,2,3,4-tetrahydroacridin-9-amine (**12**) (232 mg, 0.765 mmol, 95 %) was obtained as a brown oil. LC-MS analysis: t_r = 5.84 min, ESI-MS: *m/z* calcd for $C_{20}H_{22}N_3$ $[M+H]^+$: 304.18, found 304.15. ^{1}H-NMR (400 MHz, CD_3OD): δ = 8.11 (d, *J* = 10.4 Hz, 1H, CH), 7.73–7.70 (m, 1H, CH), 7.58 (t, *J* = 7.5 Hz, 1H, CH), 7.32 (t, *J* = 10.4 Hz, 1H), 7.02 (d, *J* = 8.3 Hz, 2H, CH), 6.67 (d, *J* = 7.9 Hz, 2H, CH), 4.64 (s, 2H, CH_2), 3.35 (s, 2H, NH_2) 2.98–2.92 (m, 2H, CH_2), 2.68–2.63 (m, 2H, CH_2), 1.90–1.80 (m, 4H, CH_2) ppm. ^{13}C-NMR (100 MHz, CD_3OD): δ = 155.0 (1C, C_q), 154.4 (1C, C_q), 148.2 (1C, C_q), 146.2 (1C, C_q), 145.9 (1C, C_q), 130.8 (1C, CH), 129.3 (2C, CH), 125.3 (1C, CH), 125.1 (1C, CH), 123.4 (1C, CH), 116.7 (2C, CH), 116.4 (1C, C_q), 110.8 (1C, C_q), 52.9 (1C, CH_2), 33.0 (1C, CH_2), 25.7 (1C, CH_2), 23.7 (1C, CH_2), 23.2 (1C, CH_2) ppm.

4-(4-Nitrophenyl)but-3-yn-1-ol (15)

1-Brom-4-nitrobenzene (**13**) (600 mg, 2.97 mmol), PPh_3 (195 mg, 0.742 mmol), CuI (9.62 mg, 50.2 μmol) and $Pd(PPh_3)_2Cl_2$ (104 mg, 0.149 mmol) were dissolved in degassed NEt_3/THF (3:2) (10 mL) under argon-atmosphere. 3-Butin-1-ol (**14**) (899 μL, 11.9 mmol) was added and the mixture was stirred at 60 °C for 18 h. After cooling down, EtOAc was added and the organic layer was washed with H_2O, sat. $NaHCO_{3\ aq}$, brine, dried over Na_2SO_4 and the solvent was removed under reduced pressure. The crude product was purified using column chromatography (PE→PE:EtOAc (2:1)) to obtain 4-(4-nitrophenyl)but-3-yn-1-ol (**15**) (484 mg, 2.53 mmol, 85%) as orange oil. LC-MS analysis: $t_r = 8.65$ min, ESI-MS: *m/z* calcd for $C_{10}H_{10}NO_3$ $[M+H]^+$:192.07, not found. ^{1}H-NMR (400 MHz, $CDCl_3$): δ = 8.12 (d, *J* = 8.5 Hz, 2H, CH), 7.51 (d, *J* = 8.6 Hz, 2H, CH), 3.83 (t, *J* = 6.3 Hz, 2H, CH_2), 2.70 (t, *J* = 6.5 Hz, 2H, CH_2) ppm. ^{13}C-NMR (100 MHz, $CDCl_3$): δ = 146.9 (1C, C_q), 132.5 (2C, CH), 130.6 (1C, C_q), 123.6 (2C, CH), 92.9 (1C, C_q), 80.7 (1C, C_q), 60.9 (1C, CH_2), 23.8 (1C, CH_2) ppm.

4-(4-Aminophenyl)butan-1-ol (16)

4-(4-Nitrophenyl)but-3-yn-1-ol (**15**) (388 mg, 2.03 mmol) was dissolved in MeOH (10 mL). The mixture was stirred over Pd/C under H_2-atmosphere (10 bar) for 3 h. The mixture was filtrated over celite and the solvent was evaporated under reduced pressure. 4-(4-Aminophenyl)butan-1-ol (**16**) (341 mg, 2.03 mmol, quant.) was obtained as off-white solid. Mp: 73 °C. LC-MS analysis: $t_r = 4.29$ min, ESI-MS: *m/z* calcd for $C_{10}H_{16}NO$ $[M+H]^+$: 166.13, found 166.20. ^{1}H-NMR (400 MHz, $CDCl_3$): δ = 6.97 (d, *J* = 8.2 Hz, 2H, CH), 6.64–6.60 (m, 2H, CH), 3.62 (d, *J* = 6.2 Hz, 2H, CH_2), 2.53 (t, *J* = 7.3 Hz, 2H, CH_2), 1.70–1.52 (m, 6H, CH_2/NH_2) ppm. ^{13}C-NMR (100 MHz, $CDCl_3$): δ = 144.2 (1C, C_q), 132.6 (1C, C_q), 129.3 (2C, CH), 115.4 (2C, CH), 62.9 (1C, CH_2), 34.8 (1C, CH_2), 32.4 (1C, CH_2), 27.9 (1C, CH_2) ppm.

4-(4-(Phenyldiazenyl)phenyl)butan-1-ol (17)

4-(4-Aminophenyl)butan-1-ol (**16**) (931 mg, 5.64 mmol) and nitrosobenzene (664 mg, 6.20 mmol) were dissolved in AcOH (40 mL) and stirred for 18 h at RT. The mixture was basified with 2 M NaOH and the product was extracted with EtOAc. The organic layer was washed with sat. $NaHCO_{3\ aq}$, brine and dried over Na_2SO_4. The solvent was evaporated under reduced pressure and the crude product was purified using column chromatography (CH_2Cl_2→ CH_2Cl_2:MeOH:NH_3 (60:1:0.1)) to obtain 4-(4-(phenyldiazenyl) phenyl)butan-1-ol (**17**) (955 mg, 3.76 mmol, 67%) as red-orange oil. LC-MS analysis: $t_r = 10.55$ min, ESI-MS: *m/z* calcd for $C_{16}H_{19}N_2O$ $[M+H]^+$: 255.15, found 255.15. ^{1}H-NMR (400 MHz, $CDCl_3$): δ = 7.94 (t, *J* = 8.0 Hz, 2H, CH), 7.89 (d, *J* = 8.2 Hz, 2H, CH), 7.53 (t, *J* = 7.3 Hz, 2H, CH), 7.50–7.44 (m, 1H, CH), 7.34 (d, *J* = 8.2 Hz, 2H, CH), 3.65 (t, *J* = 6.7 Hz, 2H, CH_2), 2.87 (m, 1H, OH), 2.72 (t, *J* = 7.6 Hz, 2H, CH_2), 1.80–1.68 (m, 2H, CH_2), 1.69–1.57 (m, 2H, CH_2) ppm. ^{13}C-NMR (100 MHz, $CDCl_3$): δ = 152.8 (1C, C_q), 151.0 (1C, C_q), 146.1 (1C, C_q), 130.8 (1C, CH), 129.2 (2C, CH), 129.1 (2C, CH), 123.0 (2C, CH), 122.8 (2C, CH), 62.4 (1C, CH_2), 35.6 (1C, CH_2), 32.2 (1C, CH_2), 27.4 (1C, CH_2) ppm.

1-(4-(4-Bromobutyl)phenyl)-2-phenyldiazene (18)

4-(4-(Phenyldiazenyl)phenyl)butan-1-ol (**17**) (500 mg, 1.97 mmol) and PPh_3 (1.55 g, 5.90 mmol) were dissolved in dry CH_2Cl_2 (10 mL). CBr_4 (1.96 g, 5.90 mg) was added and the mixture was stirred for 3 h at RT. The solvent was evaporated under reduced pressure and the crude product was purified using column chromatography (PE→PE:CH_2Cl_2 (2:1)→CH_2Cl_2) to obtain 1-(4-(4-bromobutyl) phenyl)-2-phenyldiazene (**18**) (621 mg, 1.96 mmol, 99%) as red-orange oil. LC-MS analysis: $t_r = 11.75$ min, ESI-MS: *m/z* calcd for $C_{16}H_{18}BrN_2$ $[M+H]^+$: 317.07, found 317.05. ^{1}H-NMR (400 MHz, $CDCl_3$): δ = 7.99–7.93 (m, 2H, CH), 7.92–7.87 (m, 2H, CH), 7.53–7.47 (m, 2H, CH), 7.47–7.41 (m, 1H, CH), 7.27 (d, *J* = 8.4 Hz, 2H, CH), 3.35 (t, *J* = 6.6 Hz, 2H, CH_2), 2.63 (t, *J* = 7.5 Hz, 2H, CH_2), 1.90–1.79 (m, 2H, CH_2), 1.80–1.68 (m, 2H, CH_2) ppm. ^{13}C-NMR (100 MHz, $CDCl_3$): δ = 152.8 (1C, C_q), 151.2 (1C, C_q), 145.5 (1C, C_q), 131.0 (1C, CH), 129.3 (2C, CH), 129.2 (2C, CH), 123.2 (2C, CH), 123.0 (2C, CH), 35.0 (1C, CH_2), 33.7 (1C, CH_2), 32.3 (1C, CH_2), 29.7 (1C, CH_2) ppm.

1-(4-(4-Azidobutyl)phenyl)-2-phenyldiazene (19)

1-(4-(4-Bromobutyl)phenyl)-2-phenyldiazene (**18**) (621 mg, 1.96 mmol), NaN_3 (140 mg, 2.15 mmol) and NEt_3 (546 μL, 3.92 mmol) were dissolved in dry DMF (15 mL). The mixture was stirred at 50 °C for 18 h and was then quenched by the addition of H_2O. The solvent was evaporated under reduced pressure and the crude product was purified using column chromatography (PE: EtOAc (2:1)) to obtain 1-(4-(4-azidobutyl)phenyl)-2-phenyldiazene (**19**) (480 mg, 1.72 mmol, 88%) as red oil. LC-MS analysis: t_r = 12.02 min, ESI-MS: *m/z* calcd for $C_{16}H_{18}N_5$ $[M+H]^+$: 280.06, found 280.15. ^{1}H-NMR (400 MHz, $CDCl_3$): δ = 7.91 (d, *J* = 12.0, 2H, CH), 7.87 (d, *J* = 8.2 Hz, 2H, CH), 7.56–7.43 (m, 3H, CH), 7.33 (d, *J* = 8.2 Hz, 2H, CH), 3.31 (t, *J* = 6.7 Hz, 2H, CH_2), 2.73 (t, *J* = 7.5 Hz, 2H, CH_2), 1.84–1.71 (m, 2H, CH_2), 1.72–1.61 (m, 2H, CH_2) ppm. ^{13}C-NMR (100 MHz, $CDCl_3$): δ = 152.9 (1C, C_q), 151.3 (1C, C_q), 145.5 (1C, C_q), 130.9 (1C, CH), 129.21 (2C, CH), 129.20 (2C, CH), 123.1 (2C, CH), 122.9 (2C, CH), 51.4 (1C, CH_2), 35.4 (1C, CH_2), 28.6 (1C, CH_2), 28.4 (1C, CH_2) ppm.

4-(4-(Phenyldiazenyl)phenyl)butan-1-amine (20)

1-(4-(4-Azidobutyl)phenyl)-2-phenyldiazene (**19**) (466 mg, 1.67 mmol) was dissolved in THF:H_2O (10:1) (11 mL). PPh_3 (875 mg, 3.34 mmol) was added and the mixture was stirred for 2 d at RT. The solvent was evaporated under reduced pressure and the crude product was purified using column chromatography (CH_2Cl_2→ CH_2Cl_2:MeOH:NH_3 ((60:1:0.1) → (5:1:0.1))) to obtain 4-(4-(phenyldiazenyl)phenyl)butan-1-amine (**20**) (382 mg, 1.51 mmol, 90%) as red oil. LC-MS analysis: $t_r = 8.37$ min, ESI-MS: *m/z* calcd for $C_{16}H_{20}N_3$ $[M+H]^+$: 254.17, found 254.15. ^{1}H-NMR (400 MHz, $CDCl_3$): δ = 7.95–7.89 (m, 2H), 7.86 (d, *J* = 8.3 Hz, 2H), 7.52–7.42 (m, 3H), 7.31 (d, *J* = 8.2 Hz, 2H), 2.78–2.58 (m, 6H, CH_2/NH_2), 1.68 (m, 2H, CH_2), 1.57–1.46 (m, 2H, CH_2) ppm. ^{13}C-NMR (100 MHz, $CDCl_3$): δ = 152.7 (1C, C_q), 151.0 (1C, C_q), 145.9 (1C, C_q), 130.7 (1C, CH), 129.1 (2C, CH), 129.0 (2C, CH), 122.9 (2C, CH), 122.7 (2C, CH), 41.7 (1C, CH_2), 35.5 (1C, CH_2), 32.6 (1C, CH_2), 28.4 (1C, CH_2) ppm.

Photochemical Properties

Absorption measurements were performed by Varian Cary 50 Bio UV-Visible Spectrophotometer and were analysed by CaryWinUV Software. The sample was analyzed in a cuvette (Hellma®, quartz glas Suprasil). Absorption spectra was measured at RT between 250 nm–600 nm.

Cholinesterase Inhibition

*h*BChE (E.C. 3.1.1.8, from humans) was kindly provided by Oksana Lockridge from the University of Nebraska Medical Center. *h*AChE was purchased from Sigma Aldrich. DTNB (Ellman's reagent), ATC and BTC iodides were obtained from Fluka Analytical. Tacrine as a reference compound was isolated during the synthesis as by-product (99% purity). A phosphate solution was prepared by dissolving NaH_2PO_4 in H_2O (55 mM) and adjusting a pH 8.0 by

adding 0.1 M NaOH. A 10 mM DNTB stock solution was diluted with buffer to 0.3 mM.

The stock solutions of the test compounds were prepared in DMSO (4 mM) and diluted with buffer to a starting concentration of 10 μM. To 85.6 μL of the compound solution (10 μM), 214.3 μL DNTB in buffer solution (0.3 mM) was added. This led to a concentration of 2.5 μM with 0.02% DMSO. Further desired dilutions were prepared on 96-well plate (2.5 μM–0.01 nM). Then 130 μL of each concentration of compound dilution and 10 μL enzyme were incubated for 5 min. Afterward, 3 μL ATC or BTC was added and enzyme activity was immediately observed via UV ($\lambda =$ 412 nm). Each concentration was repeated as a triplicate. The DMSO stock-solution of azo-bistacrine (**5**) was irradiated with 365 nm for an adapted time before dilution with assay buffer, while dilutions of azo(4)tacrine (**6**) in assay buffer were irradiated with 365 nm before enzyme addition. After irradiation with 365 nm, experiments were carried out in the dark. The IC_{50}-values were calculated by a sigmoidal fit $(y = A_1 + (A_2 - A_1)/(1 + 10^{((logx_0 - x)\cdot p)})$ using OriginPro, Version *2017*G SR2, OriginLab Corporation, Northampton, MA, USA.

AChE Kinetic Assay

To investigate the mechanism of *h*AChE inhibition of the compounds, double reciprocal plots of 1/*V* and 1/[S] were assessed by a similar setup as described above. Different inhibitor concentrations, depending on IC_{50} values, were prepared in buffer solution containing DTNB (0.3 mM). Triplicates of 130 μL were then incubated with 10 μL *h*AChE for 5 min at rt before 3 μL solutions of different ATC iodide concentrations (5.24 mM, 8.58 mM, 19.07 mM, 23.83 mM), resulting in final substrate concentrations of 110 μM, 180 μM, 400 μM and 500 μM, were added. Kinetic measurements over 3 min at 412 nm were used to calculate substrate velocity curves. To illustrate Lineweaver-Burk plots, linear regression (double reciprocal) was constructed, using GraphPad Prism 5 software. Overlaid plots were then compared to theoretical trends for competitive, mixed-type, and non-competitive inhibition.

Acknowledgements

*We thank C. Sotriffer (Julius-Maximilians Universität Würzburg) for comments and suggestions on the modelling part of this study. We thank O. Lockridge (University of Nebraska Medical Center) for providing h*BChE. Financial support by the German Research Foundation (Deutsche Forschungsgemeinschaft) under DFG DE1546/6-3 and the European Cooperation in Science and Technology (COST) under the COST action CA15135 (MuTaLig) is gratefully acknowledged. The Elite Network of Bavaria ("Elitenetzwerk Bayern") is acknowledged for awarding a PhD position to P. Spatz within the International Doctoral Program "Receptor Dynamics". Open access funding enabled and organized by Projekt DEAL.

Conflict of Interest

The authors declare no conflict of interest.

Keywords: azobenzenes · enzymes · kinetics · photopharmacology · tacrine

[1] W. A. Velema, W. Szymanski, B. L. Feringa, *J. Am. Chem. Soc.* **2014**, *136*, 2178–2191.
[2] K. Hüll, J. Morstein, D. Trauner, *Chem. Rev.* **2018**, *118*, 10710–10747.
[3] a) W. Szymański, J. M. Beierle, H. A. V. Kistemaker, W. A. Velema, B. L. Feringa, *Chem. Rev.* **2013**, *113*, 6114–6178; b) J. Broichhagen, J. A. Frank, D. Trauner, *Acc. Chem. Res.* **2015**, *48*, 1947–1960.
[4] C. Patterson, *Alzheimers Dis. Int.* **2018**.
[5] a) M. L. Bolognesi, M. Bartolini, A. Cavalli, V. Andrisano, M. Rosini, A. Minarini, C. Melchiorre, *J. Med. Chem.* **2004**, *47*, 5945–5952; b) U. Košak, B. Brus, D. Knez, R. Šink, S. Žakelj, J. Trontelj, A. Pišlar, J. Šlenc, M. Gobec, M. Živin, L. Tratnjek, M. Perše, K. Sałat, A. Podkowa, B. Filipek, F. Nachon, X. Brazzolotto, A. Więckowska, B. Malawska, J. Stojan, I. M. Raščan, J. Kos, N. Coquelle, N. Colletier, S. Gobec, *Sci. Rep.* **2016**, *6*, 39495; c) A. Alzheimer, *Allgemeine Zeitschrift für Psychiatrie und Psychisch-gerichtliche Medizin.* **1907**, 146–148.
[6] L. A. Craig, N. S. Hong, R. J. McDonald, *Neurosci. Biobehav. Rev.* **2011**, *35*, 1397–1409.
[7] a) M. E. Hasselmo, J. M. Bower, *Trends Neurosci.* **1993**, *16*, 218–222; b) M. Hoffmann, C. Stiller, E. Endres, M. Scheiner, S. Gunesch, C. Sotriffer, T. Maurice, M. Decker, *J. Med. Chem.* **2019**, *62*, 9116–9140; c) Q. Li, H. Yang, Y. Chen, H. Sun, *Eur. J. Med. Chem.* **2017**, *132*, 294–309; d) D. A. Rodríguez-Soacha, M. Scheiner, M. Decker, *Eur. J. Med. Chem.* **2019**, *180*, 690–706; e) D. A. Rodríguez-Soacha, M. Decker, *Adv. Ther.* **2018**, *1*, 1800037.
[8] H. Dvir, I. Silman, M. Harel, T. L. Rosenberry, J. L. Sussman, *Chem.-Biol. Interact.* **2010**, *187*, 10–22.
[9] J. S. Birks, *Cochrane Database Syst. Rev.* **2006**, 1465–1858.
[10] a) M. Bartolini, C. Bertucci, V. Cavrini, V. Andrisano, *Biochem. Pharmacol.* **2003**, *65*, 407–416; b) S. Varadarajan, S. Yatin, M. Aksenova, D. A. Butterfield, *J. Struct. Biol.* **2000**, *130*, 184–208.
[11] a) M.-S. García-Allón, D. H. Small, J. Avila, J. Sáez-Valero, *Front. Mol. Neurosci.* **2011**, *4:* 22; b) M.-X. Silveyra, M.-S. García-Ayllón, E. G. de Barreda, D. H. Small, S. Martínez, J. Avila, J. Sáez-Valero, *Neurobiol. Aging* **2012**, *33*, 624.e23–34.
[12] a) X. Chen, S. Wehle, N. Kuzmanovic, B. Merget, U. Holzgrabe, B. König, C. A. Sotriffer, M. Decker, *ACS Chem. Neurosci.* **2014**, *5*, 377–389; b) L. Piazzi, A. Rampa, A. Bisi, S. Gobbi, F. Belluti, A. Cavalli, M. Bartolini, V. Andrisano, P. Valenti, M. Recanatini, *J. Med. Chem.* **2003**, *46*, 2279–2282.
[13] a) P. Stawski, M. Sumser, D. Trauner, *Angew. Chem. Int. Ed.* **2012**, *51*, 5748–5751; *Angew. Chem.* **2012**, *124*, 5847–5850; b) P. Stawski, M. Sumser, D. Trauner, *Angew. Chem.* **2012**, *124*, 5847–5850; *Angew. Chem. Int. Ed.* **2012**, *51*, 5748–5751; c) M. Stein, S. J. Middendorp, V. Carta, E. Pejo, D. E. Raines, S. A. Forman, E. Sigel, D. Trauner, *Angew. Chem. Int. Ed.* **2012**, *51*, 10500–10504; *Angew. Chem.* **2012**, *124*, 10652–10656; d) M. Stein, S. J. Middendorp, V. Carta, E. Pejo, D. E. Raines, S. A. Forman, E. Sigel, D. Trauner, *Angew. Chem.* **2012**, *124*, 10652–10656; *Angew. Chem. Int. Ed.* **2012**, *51*, 10500–10504; e) W. A. Velema, W. Szymanski, B. L. Feringa, *J. Am. Chem. Soc.* **2014**, *136*, 2178–2191; f) W. A. Velema, M. C. Stuart, W. Szymanski, B. L. Feringa, *Chem. Commun.* **2013**, *49*, 5001–5003; g) W. A. Velema, M. Van der Toorn, W. Szymanski, B. L. Feringa, *J. Med. Chem.* **2013**, *56*, 4456–4464.
[14] a) J. Broichhagen, I. Jurastow, K. Iwan, W. Kummer, D. Trauner, *Angew. Chem. Int. Ed.* **2014**, *53*, 7657–7660; *Angew. Chem.* **2014**, *126*, 7788–7792; b) J. Broichhagen, I. Jurastow, K. Iwan, W. Kummer, D. Trauner, *Angew. Chem.* **2014**, *126*, 7788–7792; *Angew. Chem. Int. Ed.* **2014**, *53*, 7657–7660.
[15] a) Y.-P. Pang, P. Quiram, T. Jelacic, F. Hong, S. Brimijoin, *J. Biol. Chem.* **1996**, *271*, 23646–23649; b) A. Minarini, A. Milelli, V. Tumiatti, M. Rosini, E. Simoni, M. Bolognesi, V. Andrisano, M. Bartolini, E. Motori, C. Angeloni, *Neuropharmacology* **2012**, *62*, 997–1003.
[16] B. Biscussi, M. A. Sequeira, A. P. Murray, *Proceedings* **2019**, *41*, 80.
[17] a) L. Agnetta, M. Kauk, M. C. A. Canizal, R. Messerer, U. Holzgrabe, C. Hoffmann, M. Decker, *Angew. Chem. Int. Ed.* **2017**, *56*, 7282–7287; *Angew. Chem.* **2017**, *129*, 7388–7393; b) L. Agnetta, M. Kauk, M. C. A. Canizal, R. Messerer, U. Holzgrabe, C. Hoffmann, M. Decker, *Angew. Chem.* **2017**, *129*, 7388–7393; *Angew. Chem. Int. Ed.* **2017**, *56*, 7282–7287.
[18] E. H. Rydberg, B. Brumshtein, H. M. Greenblatt, D. M. Wong, D. Shaya, L. D. Williams, P. R. Carlier, Y. P. Pang, I. Silman, J. L. Sussman, *J. Med. Chem.* **2006**, *49*, 5491–5500.

[19] T. L Rosenberry, X. Brazzolotto, I. R. Macdonald, M. Wandhammer, M. Trovaslet-Leroy, S. Darvesh, F. Nachon, *Molecules* **2017**, *22*, 2098.
[20] M.-K. Hu, C.-F. Lu, *Tetrahedron Lett.* **2000**, *41*, 1815–1818.
[21] A. Antoine John, Q. Lin, *J. Org. Chem.* **2017**, *82*, 9873–9876.
[22] L. Fang, B. Kraus, J. Lehmann, J. Heilmann, Y. Zhang, M. Decker, *Bioorg. Med. Chem. Lett.* **2008**, *18*, 2905–2909.
[23] M. Scheiner, D. Dolles, S. Gunesch, M. Hoffmann, M. Nabissi, O. Marinelli, M. Naldi, M. Bartolini, S. Petralla, E. Poeta, B. Monti, C. Falkeis, M. Vieth, H. Hübner, P. Gmeiner, R. Maitra, T. Maurice, M. Decker, *J. Med. Chem.* **2019**, *62*, 9078–9102.
[24] Chemical Computing Group ULC, Motreal, QC, Canada, **2019**.
[25] I. J. Bruno, J. C. Cole, P. R. Edgington, M. Kessler, C. F. Macrae, P. McCabe, J. Pearson, R. Taylor, *Acta Crystallogr.* **2002**, *B58*, 389–397.
[26] The Pymol Molecular Graphics System, Version 2.0, Schrödinger, LLC.

Manuscript received: May 27, 2020
Revised manuscript received: August 3, 2020
Version of record online: September 7, 2020

After publication of the Early View version, the figures and schemes were exchanged with higher resolution versions, some captions were modified and minor changes made. – The Editors.